

# [AQ1] Functional Halt Positions of Rotary $F_0F_1$ -ATPase Correlated with Crystal Structures

Hendrik Sielaff, Henning Rennekamp, Siegfried Engelbrecht, and Wolfgang Junge  
Department of Biophysics, University of Osnabrück, D-49069 Osnabrück, Germany

**ABSTRACT** The  $F_0F_1$ -ATPase is a rotary molecular motor. Driven by ATP-hydrolysis, its central shaft rotates in 80° and 40° steps, interrupted by catalytic and ATP-waiting dwells. We recorded rotations and halts by means of microvideography in laboratory coordinates. A correlation with molecular coordinates was established by using an engineered pair of cysteines that, under oxidizing conditions, formed zero-length cross-links between the rotor and the stator in an orientation as found in crystals. The fixed orientation coincided with that of the catalytic dwell, whereas the ATP waiting dwell was displaced from it by +40°. In crystals, the convex side of the cranked central shaft faces an empty nucleotide binding site, as if holding it open for arriving ATP. Functional studies suggest that three sites are occupied during a catalytic dwell. Our data imply that the convex side faces a nucleotide-occupied rather than an empty site. The enzyme conformation in crystals seems to differ from the conformation during either dwell of the active enzyme. A revision of current schemes of the mechanism is proposed.

## INTRODUCTION

The  $F_0F_1$ -ATPase is composed of two rotary motor/generators with electrochemical, mechanical, and chemical functions. It is unique in that the procession over the angular reaction coordinate can be followed by direct observation in the microscope of single molecules (1,2), and interpreted in terms of crystal structures (3–5) with up to 1.9-Å resolution (6). The former approach reveals dynamic behavior in laboratory (i.e., macroscopic) coordinates, whereas the latter [AQ3] shows stills of certain conformations in molecular coordinates. Here, we aim at gauging microscopically detected motion in terms of molecular coordinates.

We used the holoenzyme of *Escherichia coli*,  $EF_0F_1$ . The peripheral  $EF_1$  (subunits  $\alpha_3\beta_3\gamma\delta\epsilon$  in *E. coli*) processes ADP/P<sub>i</sub> or ATP, and the membrane integral  $EF_0$  (subunits  $ab_2c_{10}$  in *E. coli*) translocates ions. Both portions are stepping rotary engines. The eight different subunits are either attributed to the “rotor” (subunits  $\gamma$  and  $\epsilon$  of  $F_1$  plus  $c_{10}$  of  $F_0$ ) or to the “stator” (subunits  $\alpha_3$ ,  $\beta_3$ , and  $\delta$ , of  $F_1$ , plus subunits  $a$  and  $b_2$  of  $F_0$ ) (7–10) (Fig. 1 A).


The crystal structure of the homologous bovine mitochondrial  $F_1$  ( $MF_1$ ) reveals a threefold pseudosymmetry of  $(\alpha\beta)_3\gamma$ , with three catalytic nucleotide binding sites. Located mainly on  $\beta$  at the interface with  $\alpha$ , they differ in their occupancy. One site is empty ( $\beta_E$ ) (3), one contains ADP-azide (4) or AMP-PNP (6) ( $\beta_D$ ), and the third contains AMP-PNP, an ATP analog ( $\beta_T$ ). The nucleotide occupancies seem to be dictated by the angular position of the central cranked shaft, subunit  $\gamma$ , and vice versa. The crystal structures of the

mitochondrial enzyme all (except for one) (11) show the convex side of  $\gamma$  facing the single unoccupied nucleotide-binding site, regardless of the presence of nonhydrolysable substrates (i.e., inhibitors) required for crystallization (5,6,12–17). It is conceived that the ~~cranked~~ coil domain of  $\gamma$ , by pushing a lever located within the C-terminal helical domain of subunit  $\beta$ , would keep this catalytic site open and empty, ready for binding of another nucleotide molecule to initiate the next step of rotary catalysis.

The microvideographic rotation assay of ATP hydrolysis by  $F_1$  of a thermophilic bacterium,  $TF_1$ , revealed the rotation of the central shaft, subunit  $\gamma$  (1). Its steps are interrupted by halts. The duration of the “ATP-waiting dwell” depends on ATP concentration, and is followed by a step of +80°, and by the subsequent “catalytic dwell” by another step of +40°, and so forth, with a period of 120° (18–20) (positive angles denote “hydrolysis direction”, i.e., counterclockwise when viewed from the membrane). The catalytic dwell is composed of at least two partial reactions without change of rotor position (18). A recent study of catalytic cooperativity between three catalytic sites revealed the influence of one particular site (altered by mutation) on events carried out by the other two, and this led the authors to propose an asymmetric sequential mechanism where three sites are occupied during the catalytic dwell (21). This finding is compatible with those of earlier studies where, under saturating concentrations of ATP, a threefold nucleotide occupancy was determined by fluorescence assay (22–25). These data are also compatible with the result that one molecule of fluorescent ~~AdN~~ remains bound to the enzyme over 240° of the full reaction circle (18). [AQ4] The functional contribution of three rather than two sites to steady-state hydrolysis, however, may remain debatable (26).

The microvideographic rotation assay yields a stepped rotation in a given single molecule relative to laboratory coordinates. [AQ5] The orientation of this enzyme on a solid support

Submitted June 12, 2008, and accepted for publication August 5, 2008.

Address reprint requests to Wolfgang Junge,  Universität Osnabrück, Biologie, R.35/42, Barbarastr. 11, D-49076 Osnabrück, Germany. Tel.: 49-541-969-2872; Fax: 49-541-969-12872; E-mail: junge@uos.de.

[AQ2] Siegfried Engelbrecht's present address is the Dept. of Biochemistry, University of Osnabrück, D-49069 Osnabrück, Germany.

Editor: Klaus Schulten.

© 2008 by the Biophysical Society  
0006-3495/08/11/1/09 \$2.00

doi: 10.1529/biophysj.108.139782

is unknown, however, and this has prevented the correlation of dwells and moves with ~~molecular coordinates~~. To find out how the ATP-waiting dwell and the catalytic dwell are related to crystal structure, we studied the stepped rotation in a mutant of EF<sub>0</sub>F<sub>1</sub> under reducing conditions, and marked a rotor/stator configuration, as in crystal structures, by oxidizing appropriately engineered pairs of cysteines to form a disulfide bridge as a zero-length cross-link between rotor and stator.

Single-pair fluorescence resonance energy transfer was previously used to correlate crystal structure with macroscopic observables (27). The precision of this approach is limited by: 1), the necessity to guess position in the structure of one reporter dye; 2), a long linker length (1.2 nm and 1.7 nm); and 3), ad hoc assumptions regarding dye mobility. Here, these limitations were overcome by zero-length cross-links between rotor and stator.

## MATERIALS AND METHODS

### Reagents

Reagents were purchased from Biomol (Hamburg, Germany), Bio-Rad (Munich, Germany), Fluka (Buchs, Switzerland), IBA (Göttingen, Germany), New England Biolabs (Frankfurt am Main, Germany), Qiagen (Hilden, Germany), Ridel de Haëen (Seelze, Germany), Roche (Mannheim, Germany), Roth (Karlsruhe, Germany), and Sigma (Taufkirchen, Germany), and were of the highest grade available.

### Molecular genetics

The plasmid pSE1 (all wild-type cysteines substituted by alanines, His<sub>6</sub> tag N-terminal at subunit β, Strep tag C-terminal in subunit c) (28) was used as the starting plasmid. For the αE284C, αD336C, γL276C, γQ274C, and γK266C mutations, pBluescript II SK (±) subclones were generated by insertion of the *KpnI/XhoI* and *KpnI/SacI* fragments of pSE1. Site-directed mutagenesis performed via polymerase chain reaction, using the oligonucleotide 5'-CGCCAGGACGTTGTGCATTCCCGG-3' and its complement 5'-CCGGGAATGCACAACGTCCTGGCG-3' for αE284C, 5'-CGAACTCAGGCGGGTGTGTTCTGCGTTCGTTCC-3' and its complement 5'-GGAACGAACGCAGAAACACAACCCGCCTGAGTTTCG-3' for αD336C, 5'-GCATTACTCAGGAATGCACCG AGATCGTCTCG-3' and its complement 5'-CGAGACGATCTCGGTGCATTCTGAGTAA TGC-3' for γL276C, 5'-GCTCGTCAGGCCAGCATTACTGTGAACATCCAGAG-ATCGT CTGC-3' and its complement 5'-CGAGACGATCTCGGTGAG-TTACAAGTAATGCTGGCCTGACGAGC-3' for γQ274C, and 5'-GCA-GTTGGTATACAACCTGTGCTCGTCAGGCC AGC-3' and its complement 5'-GCTGGCCTGACGAGCACAGTTGTATACCAACTGC-3' for γK266C (29). The *KpnI/XhoI* fragments of pSE1 were substituted with the corresponding fragments carrying the αE284C or αD336C mutations by standard restriction and ligation, resulting in plasmids pKG7 and pMM34, respectively. The double mutants αE284C/γL276C, αE284C/γQ274C, and αD336C/γK266C were then generated by exchanging the *KpnI/SacI* fragment of pKG7 and pMM34 with the corresponding mutated fragments by standard restriction and ligation, resulting in the plasmids pGH14, pGH18, and pGH11, respectively. Successful cloning was checked by nucleotide sequencing.

### Preparation of EF<sub>0</sub>F<sub>1</sub>

The *E. coli* strain DK8 (30) was transformed with pSE1, pGH11, pGH14, or pGH18. Cells were collected at OD<sub>600</sub> = 0.8. Membranes were purified

essentially according to Wise (31). The procedure included two additional washing steps with 5 mM Tris-HCl (pH 8), 10 mM MgCl<sub>2</sub>, 0.2 mM EGTA, and 10% (v/v) glycerol, followed by centrifugation at 220,000 × g for 90 min. Membrane pellet aliquots were stored (20 mg protein/mL in 5 mM Tris-HCl (pH 8), 10 mM MgCl<sub>2</sub>, 70 mM KCl, and 20% (v/v) glycerol) at -80°C. Membranes (100 mg protein) were suspended at 5 mg/mL protein in 50 mM Tris-HCl (pH 7.5), 5 mM, 1 mM K-ADP, and 15% glycerol plus one tablet of Boehringer complete inhibitor tablets/50 mL extraction volume. We added *N*-octyl-L-D-glucopyranoside (25% (w/v) in H<sub>2</sub>O) dropwise to an initial concentration of 1%. After stirring for 15 min on ice, additional detergent was added, to a final concentration of 2.2% (w/v). Membrane protein was extracted by stirring on ice for 30 min, followed by centrifugation at 100,000 × g for 90 min. Avidin was added (1 μg/mL), followed by dilution of the supernatant to 1% (w/v) *N*-octyl-L-D-glucopyranoside (Biomol) with buffer A (20 mM TES, pH 7.5, 5 mM MgCl<sub>2</sub>, 1 mM K-ADP, and 15% (v/v) glycerol). This solution was applied batchwise to 5 mL streptactin-sepharose (settled volume, 5 mg streptactin/mL). The gel was packed into an empty NAP-10 column (Pharmacia), and washed with 5 mL buffer A containing 1% (w/v) *N*-octyl-L-D-glucopyranoside at 0.5 mL/min. The EF<sub>0</sub>EF<sub>1</sub> was then eluted with 10 mL of the same buffer containing 2.5 mM desthiobiotin. Protein determination was performed according to Sedmak and Grossberg (32). Seventy percent glycerol was added to the eluates before they were quick-frozen in liquid nitrogen and stored at -80°C before use.

### Cross-linking of EF<sub>0</sub>F<sub>1</sub> mutants

The EF<sub>0</sub>F<sub>1</sub> preparations were treated with 100 μM DTT or 10 mM DTT for 2 h at ambient temperature, to oxidize or reduce introduced cysteine residues. The quantitative formation of cross-links was checked by polyacrylamide gel electrophoresis in the presence of SDS (12.5%), followed by Western blotting overnight at 4°C. Polyclonal primary mouse antibodies against α and γ were a kind gift of G. Deckers-Hebestreit (Department of Microbiology, University of Osnabrück, Osnabrück, Germany) and S. D. Dunn (Department of Biochemistry, University of Western Ontario, London, Ontario, Canada), respectively. After incubation with secondary monoclonal anti-mouse antibodies for 60 min, bands were detected with the Lumi-Light<sup>Plus</sup> Western Blotting Kit (Roche). [A06] [A07]

### Preparation of F-actin

The G-actin was prepared from acetone powder obtained from rabbit skeletal muscle, as described by Pardee and Spudich (33). The protein was briefly sonified and gel-filtrated against 2 mM MOPS/KOH (pH 7.0), 0.2 mM CaCl<sub>2</sub>, and 2 mM ATP (buffer B). Biotinylation was performed with a six-fold molar excess of biotin-PEAC<sub>5</sub>-maleimide (Dojindo Laboratories) for 2 h at ambient temperature. Excess reagent was removed by an overnight dialysis (buffer B), followed by two successive gel filtrations (GE Healthcare PD 10/buffer B). This preparation was stored frozen in aliquots at -80°C. Before use, G-actin (18 μM) was converted into fluorescently labeled F-actin by the addition of 20 mM MOPS/KOH (pH 7.0), 100 mM KCl, 10 mM MgCl<sub>2</sub>, and 18 μM phalloidin-tetramethylrhodamine-B-isothiocyanate-conjugate (Sigma) (3 h/4°C) (1). Special care was taken in pipetting the labeled F-actin. Filament length varied between 0.4–3 μm, depending on the applied shear forces. [A08]

### Immobilization of EF<sub>0</sub>F<sub>1</sub>

Samples were filled into flow cells consisting of two coverslips (bottom, 26 × 76 mm<sup>2</sup>; top, 24 × 24 mm<sup>2</sup>), separated by double-adhesive tape. Protein solutions were infused in the following order (50 μL per step, 4-min incubation) (1): 0.8 μM Ni<sup>2+</sup>-NTA-horseradish peroxidase conjugate (Qiagen) in 50 mM MOPS/KOH (pH 7.5), 50 mM KCl, 5 mM MgCl<sub>2</sub>, 0.5% (w/v) *N*-octyl-L-D-glucopyranoside, 10% (v/v) glycerol (buffer C) (2); 10 mg/mL bovine serum albumin in buffer C (3); wash with buffer C (4); 5 μM EF<sub>0</sub>EF<sub>1</sub> in buffer C (5); wash with buffer C (6); 0.5 μM streptactin in buffer C (7); wash with buffer C

(8); 200 nM biotinylated, fluorescently labeled F-actin in buffer C (7-min incubation) (9); wash with buffer C (10); 20 mM glucose, 0.2 mg/mL glucose oxidase, 50  $\mu$ g/mL catalase, 0.5% 2-mercaptoethanol, 0.2 mg/mL creatine kinase, 2.5 mM creatine phosphate, and 50  $\mu$ M ATP in buffer C. For ADP inhibition, 50  $\mu$ L of 20 mM glucose, 0.2 mg/mL glucose oxidase, 50  $\mu$ g/mL catalase, 0.5% 2-mercaptoethanol, 1 U/ $\mu$ L hexokinase, and 5 mM ADP in buffer C were added after washing with 50  $\mu$ L of buffer C. For oxidization, 50  $\mu$ L of 20 mM glucose, 0.2 mg/mL glucose oxidase, 50  $\mu$ g/mL catalase, 0.2 mg/mL creatine kinase, 2.5 mM creatine phosphate, 2 mM Ellman's reagent, and 5 mM ATP in buffer C were added after washing with 50  $\mu$ L of buffer C.

## Video microscopy

- [AQ9] An inverted fluorescence microscope (IX70, Olympus, Japan, with lens PlanApo 100U/1.40 oil, fluorescence cube) was equipped with a silicon-intensified tube camera (C 2400-08, Hamamatsu, Japan) and connected to a VHS-PAL video recorder (25 frames/s). With this setup, filaments of 5- $\mu$ m length appeared as 3-cm-long rods on a 14-inch monitor. The flow cell was loaded with samples of EF<sub>0</sub>EF<sub>1</sub> and labeled with actin filaments, and single-molecule rotation was recorded. Fast bleaching of fluorescently labeled actin filaments in the oxidized state was overcome by reducing the excitation intensity. Video data were captured with a Pinnacle DV500 Plus video card, and digitized with Adobe Premiere 6.0. A software for evaluation of the obtained video sequences was written with MATLAB 7 (The MathWorks, Natick, MA).

## Homology modeling

Our model of EF<sub>1</sub> was based on the structure determined by Abrahams et al. (3) (1bmf). Modeling was performed with the program WhatIf (34,35). The model coordinates are available from <http://www.biologie.uni-snaabrueck.de/Biochemie/Engelbrecht/sc/data/>.

## RESULTS

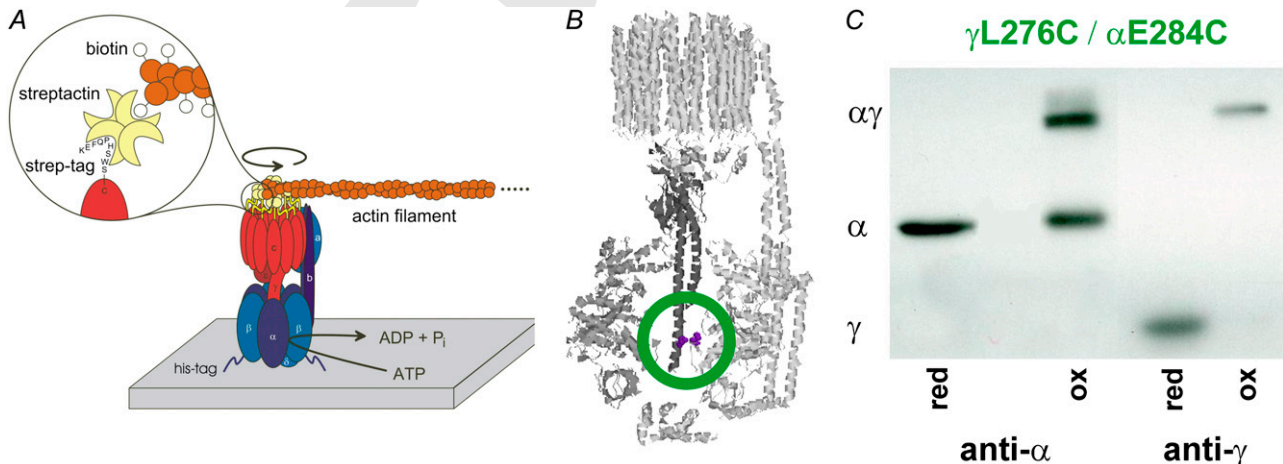
### Disulfide-locked orientations of the rotor

First we examine the reversibility, reproducibility, and phasing relative to an ADP-saturated and thereby transiently

inhibited state of EF<sub>0</sub>F<sub>1</sub>. Detergent-solubilized EF<sub>0</sub>F<sub>1</sub> was immobilized on a functionalized glass support by engineered His tags at the N-termini of the three  $\beta$ -subunits. Single-molecule rotation was recorded via a fluorescent actin filament attached to EF<sub>0</sub>-c<sub>10</sub> by a biotin/streptactin linkage to engineered Strep tags at the C-termini of EF<sub>0</sub>-c (Fig. 1 A) (28). The ATP hydrolysis-driven rotation of c<sub>10</sub> and the locked positions of the rotor were recorded by microvideography. Short filaments (0.4–1  $\mu$ m) were used to avoid viscous overdamping of the stepped rotation (36,37). Oxidizing conditions promoted the formation of a disulfide bridge between appropriately engineered cysteines (e.g.,  $\gamma$ L276C/ $\alpha$ E284C; Fig. 1 B), and blocked the rotation. It was resumed upon reduction (data not shown). The extent of cross-link formation under oxidizing conditions was nearly quantitative, as checked by SDS-PAGE and Western blotting (Fig. 1 C). In experiments with cysteine-less EF<sub>0</sub>F<sub>1</sub>, the rotation was insensitive to oxidation.

The ADP-saturated state of the enzyme was chosen as an intrinsic reference for blocking the rotation. It was distinguished by two properties: 1), the block was reversible and could be relieved by the addition of ATP; and 2), the ADP-blocked-relieved-blocked position of the rotor was reproducible within the enzyme's periodicity of 120°. We did not a priori associate the ADP-saturated state with any known structural state of the enzyme. Here it served only as an intrinsic reference to correlate the two dwells of the active enzyme (ATP-wait and catalytic) with either of the three disulfide-locked states. The rotor position during ADP-saturation was arbitrarily set at 0°, and the supposedly disulfide-locked orientations were compared with this intrinsic reference, using the following approach. After selecting an actively rotating single molecule in the presence of 50  $\mu$ M ATP, ADP inhibition was elicited by perfusing the reaction

[AQ13]



- [AQ17] FIGURE 1 Rotation assay with EF<sub>0</sub>F<sub>1</sub> and disulfide lock between rotor and stator. (A) Attachment of EF<sub>0</sub>F<sub>1</sub> by His tags on a functionalized glass support, and attachment of a fluorescent actin filament to c-ring by engineered Strep tags via streptactin/biotin (28). (B) Location of disulfide bond (in green circle) in a model of EF<sub>0</sub>F<sub>1</sub>-mutant  $\gamma$ L276C/ $\alpha$ E284C. (C) Western blot with antibody against subunits  $\alpha$  and  $\gamma$  shows almost complete formation of  $\gamma$ - $\alpha$  dimers, if mutant  $\gamma$ L276C/ $\alpha$ E284C is exposed to oxidizing conditions.



chamber with 5 mM ADP, 1 U/ $\mu$ L hexokinase, and 20 mM glucose (to eliminate ATP rapidly). The rotation was brought to a halt within  $\sim$ 10 s after starting the perfusion. The angular probability distribution of short filaments attached to the rotor was analyzed. In the ADP-saturated state, the distribution was approximately Gaussian, with the same width from one single molecule to the other. The distribution shown in yellow in Fig. 2 A represents the average over seven single molecules in their ADP-saturated state. Individual histograms were averaged after phasing by cross-correlation. Their respective peak positions were set at 0°. This peak position served as the reference zero for all other assignments. Angular positions deviating from this zero position were counted positive in the direction of hydrolysis (counterclockwise if the enzyme is viewed from the membrane side).

After recording the ADP-locked orientation for any given single molecule, the solution (containing ADP) was exchanged against 5 mM ATP, 0.2 mg/mL creatine kinase, and 2.5 mM phosphocreatine to remove ADP and relieve ADP-saturation, such that the enzyme resumed rotation within 1 min after starting the perfusion. Then we added 2 mM Ellman's reagent. It oxidized the cysteines to cystine, thus halting the rotor again within some minutes. With mutant  $\gamma$ L276C/ $\alpha$ E284C, the disulfide-locked orientation either coincided with or was rotated by 120° (Fig. 2 A, green), 240°, and so on, according to the functional C<sub>3</sub>-symmetry of F<sub>1</sub>. The coincidence within the period of 120° of halts observed during ADP-saturation and upon disulfide-blocking in the mutant  $\gamma$ L276C/ $\alpha$ E284C was observed in all single molecules in this series of experiments.

We checked two other mutants,  $\gamma$ Q274C/ $\alpha$ E284C and  $\gamma$ K266C/ $\alpha$ D336C, where we expected this coincidence to be broken. In the former, the cysteine on the rotor was displaced by 200° around the  $\alpha$ -helical wheel of subunit  $\gamma$ , whereas the cysteine on subunit  $\alpha$  of the stator remained the same. As expected, the halt positions caused by oxidation were now displaced by 40°, 160° (Fig. 2 A, orange), or 280° relative to the position during ADP-saturation (Fig. 2 A, yellow). Subunit  $\gamma$  had to rotate by 40° to react  $\gamma$ Q274C with the

nearest partner cysteine on subunit  $\alpha$  at 240°. In the third mutant,  $\gamma$ K266C/ $\alpha$ D336C, the halt position by oxidation was displaced by +105° (documented in Fig. 2 A, cyan), +225°, and so on. Fig. 2, B–D, illustrates the positions of the above three cysteine pairs in the *E. coli* homology structure, as based on the first asymmetric structure of MF<sub>1</sub> (3). Fig. 2, B–D, shows the plausibility of these displacements between the ADP-saturated and respective SS-locked states. The cysteine pair which, if oxidized, most closely approximates the rotor position in crystals is  $\gamma$ L276C/ $\alpha$ E284C. Thus both the SS-locked orientation of the rotor and the coincident ADP-locked position mark a rotor/stator orientation, as in crystals.

[AQ14]

### Steps and dwells of rotating enzyme during ATP hydrolysis in relation to disulfide-locked state

Rotation trajectories were monitored typically over 1–2 min. Fig. 3 A shows three short segments of a trajectory of one particular single molecule driven by hydrolysis in the presence of 50  $\mu$ M ATP. Two modes of stepping rotation were evident, each with a typical step-width of 120°, but the phases of these two modes differed by 40° (Fig. 3 A, red and blue). During extended periods of time, one phase dominated over the other (Fig. 3 A, two left traces). In other periods, phase-jumps were frequent (Fig. 3 A, right trajectory). Fig. 3 B shows histograms of the two modes over the full trajectory, of 1.5-min duration. Jumps of 40° were in line with previously reported transitions from a catalytic into the next ATP-waiting dwell, and jumps of 80° from an ATP-waiting into the next catalytic dwell (18,19). This assignment was here corroborated as follows. By keeping the same single molecule in focus and raising the ATP concentration from 50  $\mu$ M to 5 mM, the “blue” mode was virtually eliminated. The peaks colored in red could thus be attributed to catalytic dwells, and the blue peaks could be attributed to ATP-waiting dwells. In related experiments with TF<sub>1</sub> from a thermophilic bacterium (18,19), the ATP-waiting dwell was resolved at a much lower ATP concentration (<1  $\mu$ M). Here, with the

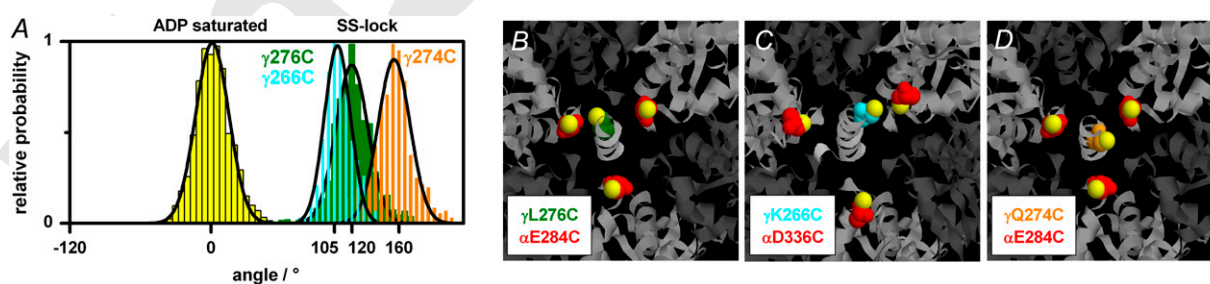


FIGURE 2 (A) Histograms of orientation of a short actin filament attached to c-ring of EF<sub>0</sub>F<sub>1</sub> in ADP-saturated state (yellow), and in disulfide-locked states of mutant enzymes  $\gamma$ L276C/ $\alpha$ E284C (green),  $\gamma$ K266C/ $\alpha$ D336C (cyan), and  $\gamma$ Q274C/ $\alpha$ E284C (orange). Starting from actively rotating single molecules (ATP-hydrolysis), rotation was halted by ADP-saturation, and angular fluctuations were recorded (yellow histogram). Rotation was resumed (perfusion with ATP), and again blocked by perfusion with oxidizing solution (green, cyan, and orange). (B–D) Cross section of homology model of EF<sub>0</sub>F<sub>1</sub> through layer of respective engineered cysteine pairs. Respective cysteines on subunit  $\alpha$  are colored in red, and those on subunit  $\gamma$  in green, cyan, or orange, as in A. Sulfur atoms are shown in yellow. For details, see text.

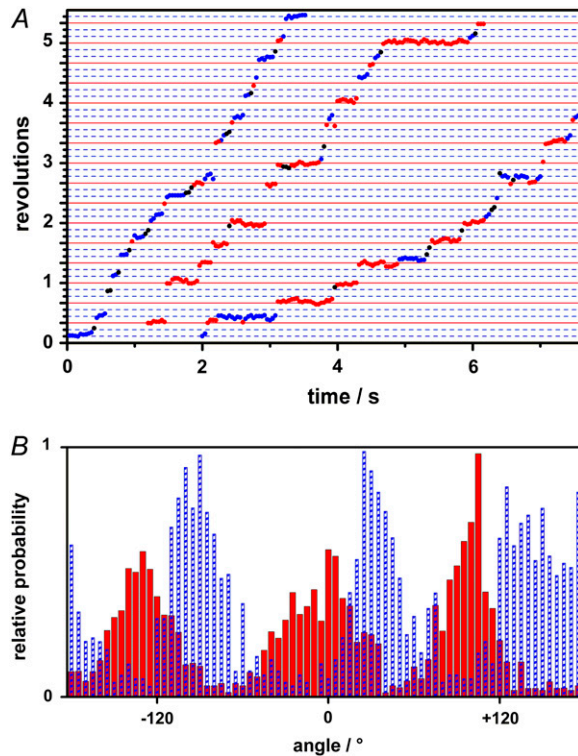


FIGURE 3 Trajectories and histograms of stepped rotation of c-ring in a single molecule of  $EF_0F_1$  double mutant  $\gamma L276C/\alpha E284C$ , as driven by the hydrolysis of 50  $\mu M$  ATP. (A) Three short segments show two modes of stepping with dwells at 120°, 240°, 360°, and so on (*red*), and at 40°, 160°, 280°, and so on (*blue*), respectively. (B) Histograms of same molecule as in A after separation of “blue” and “red” portions of total trajectory of 1.5-min duration (for attribution of “blue” peak to ATP-waiting dwell, see text).

holoenzyme from *E. coli*,  $EF_0F_1$ , it was still apparent at 50  $\mu M$  ATP, and it lasted longer ( $\sim 100$  ms). The ATP-waiting dwell of  $EF_0F_1$  was apparently controlled by an activation barrier, rather than being close to diffusion-controlled as in  $TF_1$ . We checked the phase of the catalytic and ATP-waiting dwell relative to the ADP-saturated halt by adding ADP (5 mM) to the solution over stepwise rotating single molecules.

The respective rotor positions during the catalytic dwell (*red*) and the ATP-waiting dwell (*blue*), and in the ADP-saturated state (*yellow*) and the disulfide-locked state ( $\gamma L276C/\alpha E284C$ , *green*), are summarized in Fig. 4. The angular positions of the locked enzyme, regardless of its cause (ADP saturation or disulfide-lock), coincided with the angular position of the catalytic dwell. The ATP-waiting dwell, however, was displaced by  $+40^\circ$  in the hydrolysis direction.

The duration of the ATP-waiting and catalytic halts was typically  $\sim 100$  ms. This is sufficient to relax fully both ends of the rotor, the C-terminal end of subunit  $\gamma$  in its hydrophobic bearing (3,38,39), and the c-ring with the attached short actin filament (for the elastic properties of the attached short actin filament, see Cherepanov and Junge (36)). There is no permanent distortion of the rotor (subunits  $\gamma\epsilon c_{10}$ ), and

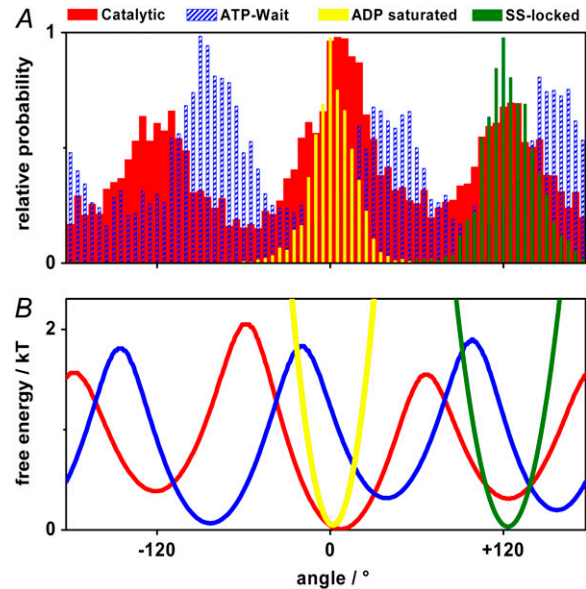


FIGURE 4 (A) Histograms of rotating (*red* and *blue*), ADP-saturated (*yellow*), and disulfide-locked (*green*) single molecules of  $EF_0F_1$ , and (B) resultant energy landscapes. Experiments were performed with double mutant  $\gamma L276C/\alpha E284C$ . Red histogram represents behavior when catalytic dwell limits overall rate, and blue histogram represents behavior when waiting for ATP limits the overall rate.

the monitored orientation of the filament attached to the  $c_{10}$ -ring (Fig. 1 A) does not deviate from the orientation of the C-terminal end carrying the disulfide-bridge (Fig. 1 B).

### Energy landscapes of stepping and of locked $EF_0F_1$

Figs. 2 A, 3 B, and 4 A show the probability distribution ( $p(\alpha)$ ) of the rotor position as a function of the angular reaction coordinate ( $\alpha$ ). In thermodynamic equilibrium, the probability distribution is related to the molecular free energy profile ( $\Delta G_0(\alpha)$ ) by Boltzmann's equation:

$$p(\alpha) = \frac{\exp\left(-\frac{\Delta G_0(\alpha)}{k_B T}\right)}{1/2\pi \int_0^{2\pi} \exp\left(-\frac{\Delta G_0(\alpha)}{k_B T}\right) d\alpha}, \quad (1)$$

where  $k_B$  denotes the Boltzmann constant, and  $T$  the absolute temperature. Maxima of the probability distribution reflect energy minima, and vice versa. Fig. 4 B shows the respective energy landscapes of  $EF_0F_1$  during the catalytic dwell (*red*), during the ATP-waiting dwell (*blue*), in the ADP-saturated state (*yellow*), and in the disulfide-locked state (mutant  $\gamma L276C/\alpha E284C$ , *green*). The fact that the observed probability distributions closely followed their Gaussian fit curves implied that the rotor fluctuated in an elastic potential well. The variance of the respective probability distributions,  $\sigma^2$ , is reciprocal to the torsional elastic spring constant,  $\kappa$ :

[AQ15]

$$\sigma^2 = \frac{k_B T}{\kappa}. \quad (2)$$

A variance of  $(13.2^\circ)^2$  of ADP-saturated  $EF_0F_1$  (Fig. 4 A, *yellow distribution*) thus implied a torsional spring constant of  $\kappa \cong 76 \text{ pN nm}$ .

## DISCUSSION

The rotary ATP-synthase  $F_0F_1$  is an extremely agile enzyme. The availability of both videos of the active enzyme and still photographs of the inhibited enzyme is unique among nature's nanomotors. The rotation of the central shaft, subunit  $\gamma$ , when driven by the hydrolysis of ATP, steps with a periodicity of  $120^\circ$  and reflects the threefold pseudosymmetry of  $F_1$ . The crystal structures of the mitochondrial enzyme show the convex side of the coiled coil portion of  $\gamma$  pointing to the single empty catalytic site; the other two sites are occupied by nucleotides. Various inhibitors were used in crystallization to lock the molecule in such an asymmetric conformation (3,5,6,11–14,16,17,40). Crystals grown in their absence produced diffuse electron density around the central shaft, indicative of low order (41–43). The asymmetric crystal structures that are taken as the common reference thus represent conformations of the inhibited enzyme. The very first, in particular, was interpreted to show the ADP-azide-inhibited state of  $F_1$  (3,4,6).

To what extent do the three disulfide cross-links trap the active *E. coli* enzyme in a conformation comparable to the one in crystals of the inhibited mitochondrial enzyme, and how large is the error? We aimed to mark the pioneering asymmetric structure of  $F_1$  (3) by appropriately engineered cysteine pairs. Disulfide bonds require a proximity of  $\sim 0.4 \text{ nm}$  between the  $C_\beta$  atoms of the respective cysteines (44,45). In the homology model of  $EF_0F_1$ , as shown in Fig. 2, *B–D*, the distance is  $\sim 50\%$  larger. Fluctuations of this distance account for the observed cross-link formation (Fig. 1 *C*). Fig. 2, *B* and *D*, also shows that disulfide bond formation in the mutants  $\gamma L276C/\alpha E284C$  and  $\gamma K266C/\alpha D336C$  requires less distortion of the crystal structure than in mutant  $\gamma Q274C/\alpha E284C$  (Fig. 2 *C*). The difference between the former two peak positions (differing by  $15^\circ$  according to Fig. 2 *A*) gives a conservative upper estimate of the absolute error, i.e.,  $\pm 7.5^\circ$ . The difference between the average peak position of the mutants  $\gamma L276C/\alpha E284C$  and  $\gamma K266C/\alpha D336C$  and the position of the mutant  $\gamma Q274C/\alpha E284C$ , i.e.,  $47.5^\circ \pm 7.5^\circ$ , is meaningful, and so is the difference between the former two and the ATP-waiting dwell. At this point, one may ask why we did not take the only crystal structure with three filled nucleotide-binding sites (11) as a reference. We refrained from doing so for two reasons: 1), This structural model shows the  $\gamma$  subunit twisted (by  $20^\circ$ ) compared with all others, and the twisted domain is located in a region of  $\gamma$  where one would have expected, in the absence of extra strain, the free rotation of the central shaft in the hydrophobic

bearing (3,38,39). 2), The mechanism of the  $F_1$ -ATPase is usually discussed in terms of the pioneering structure determined in 1994 (3), and the very similar structures with two-site occupancy that followed.

How can our data be integrated with the prevailing schemes of catalysis? Recently, a functional approach to assign a particular binding site to a catalytic event by a fluorescence quench technique was reported (22). The authors determined the proximity between a fluorescent residue at the very C-terminal region of subunit  $\gamma$  ( $\gamma L262W$ ) and MgTNT-ATP, which binds to the catalytic sites. They found the greatest quench after binding of the first nucleotide (high affinity), and additional but lesser quenching after binding of the second (medium affinity) and the third (low affinity) nucleotide. Using evidence from Baylis et al. that catalysis is mediated by the high-affinity site (46), Mao and Weber (22) concluded that the convex side of subunit  $\gamma$  points to the very nucleotide-occupied high-affinity site that is catalytically active. We would not like to go as far, because the authors could not rule out that the binding of a second nucleotide rotated  $\gamma$  such to now point to the second site or somewhere else (the additional fluorescence quench would be all the same). Marked rotational freedom of subunit  $\gamma$  under similar conditions was documented (38). In any case, Mao and Weber (22) demonstrated three-site occupancy under saturating concentration of ATP. Ariga et al. (25) arrived at a similar conclusion. In a mutated enzyme, where the kinetic properties of one  $\beta$ -subunit out of three were modified, they found that this particular site influenced the kinetics of partial reactions involving the other sites. In other words, each site governs not only its  $120^\circ$  range of the full ( $360^\circ$ ) reaction cycle, but participates in all events over the full cycle. They also arrived at the conclusion that three sites are nucleotide-occupied during the catalytic dwell(s). Both groups, by drawing arrows, designated certain orientations of the rotor in their respective reaction schemes. Both did not explicitly mention that they meant the arrow pointing to the convex side of subunit  $\gamma$ . However, if one takes the arrow to point to the convex side of subunit  $\gamma$ , our data imply that both their schemes need to be modified. In Mao and Weber (22), the rotor moves during catalytic dwells (Fig. 5 *A*), and in Ariga et al. (Fig. 5 *B*) (25), the arrow points to the empty site that is waiting for the next ATP to bind. Both versions are incompatible with our data. Taking the scheme of Mao and Weber (22) as a template, we arrived at three compatible schemes, as depicted in Fig. 5, *C–E*.

[AQ16]

The deviations of the three alternatives from the original scheme (Fig. 5 *A*) are threefold: 1), the orientation of the central shaft does not change during the catalytic dwells, i.e., before the anhydride bond is cleaved, and ADP and/or  $P_i$  is released (25); 2), the convex side of subunit  $\gamma$  as seen in crystals points to a nucleotide-occupied site during catalytic dwells; and 3), during the ATP-waiting dwell, however, the convex side of subunit  $\gamma$  is displaced by  $+40^\circ$  from its orientation—as in crystals.



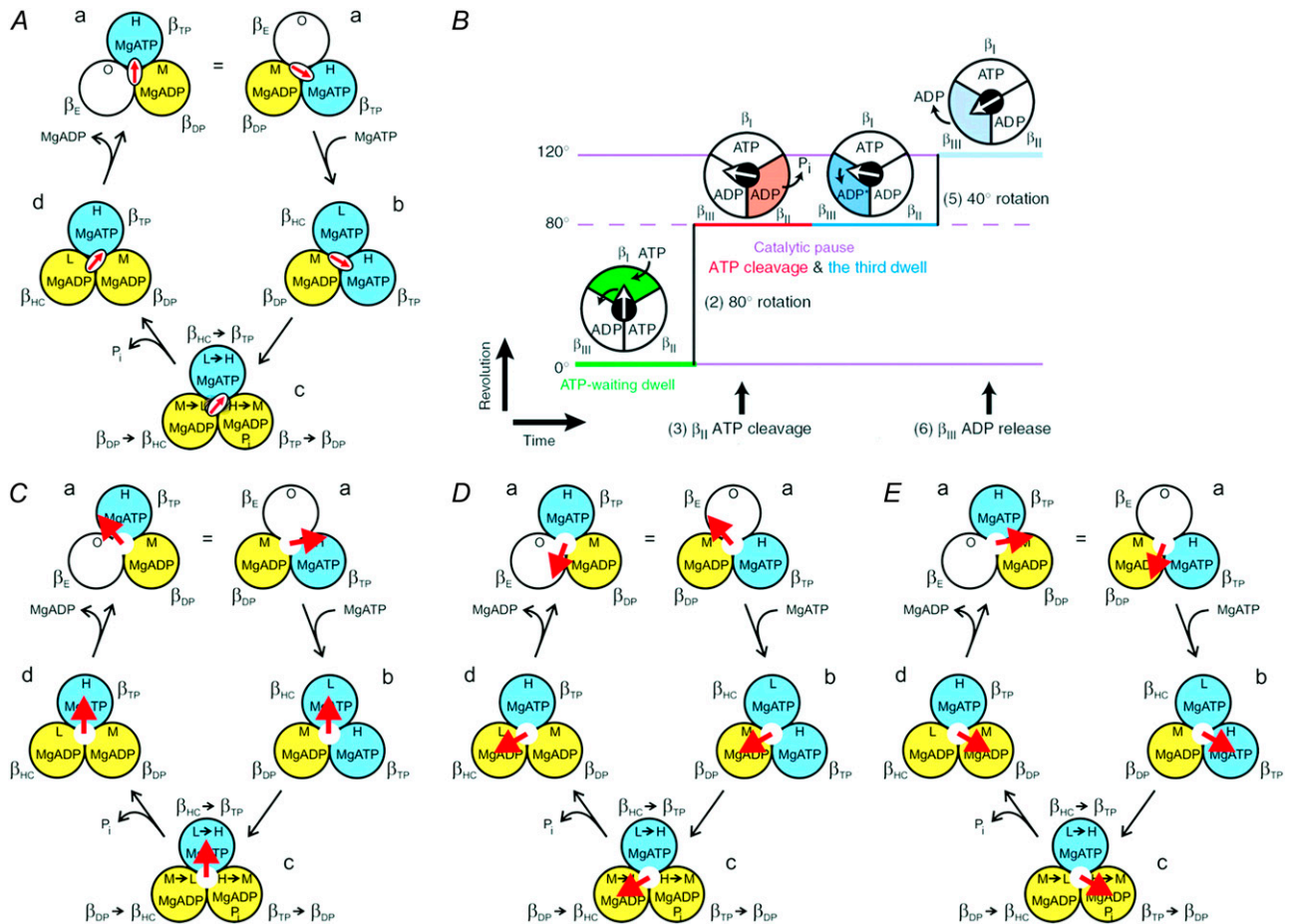


FIGURE 5 Reaction scheme of ATP-hydrolysis with catalytic dwells and ATP-waiting dwell incorporating orientation of the rotor according to this study. Arrow marks orientation of the rotor, which is apparent in crystal structures of inhibited MF<sub>1</sub> (e.g., in Abrahams et al. (3)). (A) Reaction scheme of Mao and Weber (22) (with permission of the authors). (B) Reaction scheme of Ariga et al. (25). (C–E) Modifications of the former, which are compatible with our data (see text). Four steps of 120° rotation of the rotor represent ATP-waiting dwell (a) and catalytic dwells (b–d). Red arrow symbolizes  $\gamma$ , and its tip indicates orientation of the convex side.

Because of the C<sub>3</sub>-symmetry, there is no a priori reason to discriminate between the three alternatives shown in Fig. 5, C–E. The situation in crystals, where the convex side of  $\gamma$  faces an empty nucleotide-binding site, is most closely approximated in Fig. 5 D. If one maintains the notion that the tight binding site is the catalytic one, the scheme in Fig. 5 C is most appropriate.

How do the different halt positions of the rotor of active EF<sub>0</sub>F<sub>1</sub> in this work compare with the published crystal structures of inactivated MF<sub>1</sub>? The interpretation relies on the nucleotide occupancy of the three catalytic sites in the active enzyme, and the actual participation of the sites in catalysis at any given time. This is a matter of debate (23,26). With bacterial TF<sub>1</sub>, the dependence of dwell-time on substrate concentration suggests a close-to-diffusion-controlled bimolecular reaction of ATP with a competent nucleotide-binding site (20), most probably an empty site. Experiments with active bacterial EF<sub>1</sub>, on the other hand, where occupancy was monitored via tryptophan fluorescence, showed

triple occupancy under saturating concentrations of ATP (22–24), i.e., when catalysis, but not the ATP supply, is rate-limiting, and also at saturating concentration of MgADP (47). It was evident that both the catalytic dwell and the ADP-saturated state had triple occupancy. Our data revealed the same orientation of the rotor as in the great majority of crystals of MF<sub>1</sub> during both the catalytic dwell and the ADP-saturated halt. This implied that the convex side of the rotor faced an occupied nucleotide-binding site. The rotor orientation during the ATP-waiting dwell, with one empty site, on the other hand, was displaced by +40° forward in the hydrolysis direction. The same difference by 40° between the rotor orientations of the ATP-waiting state and an “ADP-inhibited” state was previously observed in TF<sub>1</sub> (48). As it stands, the conformations of inhibited MF<sub>1</sub> as revealed by x-ray structural analysis differ from those of both the active and the ADP-saturated (ADP-inhibited) EF<sub>0</sub>F<sub>1</sub>, with the main difference that the convex side of subunit- $\gamma$  faces a nucleotide-filled site. It is conceivable that the structures published

so far of this particularly mobile enzyme were considerably affected by crystal packing forces.

The authors are very grateful for excellent technical assistance by Gaby Hikade (molecular biology) and Hella Kenneweg (single-molecule microscopy).

They acknowledge financial support by the Deutsche Forschungsgemeinschaft (SFB431/P1 to S.E.), the Volkswagen Foundation (to W.J.), the European Union (to W.J. and S.E.), and the Fonds der Chemie (to W.J.).

## REFERENCES

- Noji, H., R. Yasuda, M. Yoshida, and K. Kinosita. 1997. Direct observation of the rotation of F-ATPase. *Nature*. 386:299–302.
- Yasuda, R., H. Noji, K. Kinosita, and M. Yoshida. 1998. F<sub>1</sub>-ATPase is a highly efficient molecular motor that rotates with discrete 120° steps. *Cell*. 93:1117–1124.
- Abrahams, J. P., A. G. W. Leslie, R. Lutter, and J. E. Walker. 1994. The structure of F<sub>1</sub>-ATPase from bovine heart mitochondria determined at 2.8 Å resolution. *Nature*. 370:621–628.
- Bowler, M. W., M. G. Montgomery, A. G. Leslie, and J. E. Walker. 2006. How azide inhibits ATP hydrolysis by the F-ATPases. *Proc. Natl. Acad. Sci. USA*. 103:8646–8649.
- Braig, K., R. I. Menz, M. G. Montgomery, A. G. Leslie, and J. E. Walker. 2000. Structure of bovine mitochondrial F<sub>1</sub>-ATPase inhibited by Mg<sup>2+</sup> ADP and aluminium fluoride. *Structure*. 8:567–573.
- Bowler, M. W., M. G. Montgomery, A. G. Leslie, and J. E. Walker. 2007. Ground state structure of F<sub>1</sub>-ATPase from bovine heart mitochondria at 1.9 Å resolution. *J. Biol. Chem.* 282:14238–14242.
- Boyer, P. D. 2002. A research journey with ATP synthase. *J. Biol. Chem.* 277:39045–39061.
- Senior, A. E., S. Nadanaciva, and J. Weber. 2002. The molecular mechanism of ATP synthesis by F<sub>1</sub>F<sub>0</sub>-ATP synthase. *Biochim. Biophys. Acta*. 1553:188–211.
- Stock, D., C. Gibbons, I. Arechaga, A. G. Leslie, and J. E. Walker. 2000. The rotary mechanism of ATP synthase. *Curr. Opin. Chem. Biol.* 10:672–679.
- Junge, W., H. Lill, and S. Engelbrecht. 1997. ATP synthase: an electrochemical transducer with rotatory mechanics. *Trends Biochem. Sci.* 22:420–423.
- Menz, R. I., J. E. Walker, and A. G. Leslie. 2001. Structure of bovine mitochondrial F(1)-ATPase with nucleotide bound to all three catalytic sites: implications for the mechanism of rotary catalysis. *Cell*. 106:331–341.
- Abrahams, J. P., S. K. Buchanan, M. J. van Raaij, I. M. Fearnley, A. G. W. Leslie, and J. E. Walker. 1996. The structure of bovine F<sub>1</sub>-ATPase complexed with the peptide antibiotic efrapeptin. *Proc. Natl. Acad. Sci. USA*. 93:9420–9424.
- van Raaij, M. J., J. P. Abrahams, A. G. W. Leslie, and J. E. Walker. 1996. The structure of bovine F<sub>1</sub>-ATPase complexed with the antibiotic inhibitor aurovertin B. *Proc. Natl. Acad. Sci. USA*. 93:6913–6917.
- Orriss, G. L., A. G. W. Leslie, K. Braig, and J. E. Walker. 1998. Bovine F<sub>1</sub>-ATPase covalently inhibited with 4-chloro-7-nitrobenzofurazan—the structure provides further support for a rotary catalytic mechanism. *Structure*. 6:831–837.
- Gibbons, C., M. G. Montgomery, A. G. Leslie, and J. E. Walker. 2000. The structure of the central stalk in bovine F<sub>1</sub>-ATPase at 2.4 Å resolution. *Nat. Struct. Biol.* 7:1055–1061.
- Kagawa, R., M. G. Montgomery, K. Braig, A. G. W. Leslie, and J. E. Walker. 2004. The structure of bovine F<sub>1</sub>-ATPase inhibited by ADP and beryllium fluoride. *EMBO J.* 23:2734–2744.
- Kabaleswaran, V., N. Puri, J. E. Walker, A. G. Leslie, and D. M. Mueller. 2006. Novel features of the rotary catalytic mechanism revealed in the structure of yeast F<sub>1</sub> ATPase. *EMBO J.* 25:5433–5442.
- Nishizaka, T., K. Oiwa, H. Noji, S. Kimura, E. Muneyuki, M. Yoshida, and K. Kinosita Jr. 2004. Chemomechanical coupling in F<sub>1</sub>-ATPase revealed by simultaneous observation of nucleotide kinetics and rotation. *Nat. Struct. Mol. Biol.* 11:142–148.
- Shimabukuro, K., R. Yasuda, E. Muneyuki, K. Y. Hara, K. Kinosita Jr., and M. Yoshida. 2003. Catalysis and rotation of F<sub>1</sub> motor: cleavage of ATP at the catalytic site occurs in 1 ms before 40 degree substep rotation. *Proc. Natl. Acad. Sci. USA*. 100:14731–14736.
- Yasuda, R., H. Noji, M. Yoshida, K. Kinosita Jr., and H. Itoh. 2001. Resolution of distinct rotational substeps by submillisecond kinetic analysis of F<sub>1</sub>-ATPase. *Nature*. 410:898–904.
- Ariga, T., T. Masaïke, H. Noji, and M. Yoshida. 2002. Stepping rotation of F<sub>1</sub>-ATPase with one, two, or three altered catalytic sites that bind ATP only slowly. *J. Biol. Chem.* 277:24870–24874.
- Mao, H. Z., and J. Weber. 2007. Identification of the betaTP site in the x-ray structure of F<sub>1</sub>-ATPase as the high-affinity catalytic site. *Proc. Natl. Acad. Sci. USA*. 104:18478–18483.
- Weber, J., and A. E. Senior. 2000. ATP synthase: what we know about ATP hydrolysis and what we do not know about ATP synthesis. *Biochim. Biophys. Acta*. 1458:300–309.
- Weber, J., S. Wilke-Mounts, R. S. F. Lee, E. Grell, and A. E. Senior. 1993. Specific placement of tryptophan in the catalytic sites of *Escherichia coli* F<sub>1</sub>-ATPase provides a direct probe of nucleotide binding: maximal ATP hydrolysis occurs with three sites occupied. *J. Biol. Chem.* 268:20126–20133.
- Ariga, T., E. Muneyuki, and M. Yoshida. 2007. F<sub>1</sub>-ATPase rotates by an asymmetric, sequential mechanism using all three catalytic subunits. *Nat. Struct. Mol. Biol.* 14:841–846.
- Boyer, P. D. 2002. Catalytic site occupancy during ATP synthase catalysis. *FEBS Lett.* 512:29–32.
- Yasuda, R., T. Masaïke, K. Adachi, H. Noji, H. Itoh, and K. Kinosita Jr. 2003. The ATP-waiting conformation of rotating F<sub>1</sub>-ATPase revealed by single-pair fluorescence resonance energy transfer. *Proc. Natl. Acad. Sci. USA*. 100:9314–9318.
- Pänke, O., K. Gumbiowski, W. Junge, and S. Engelbrecht. 2000. F-ATPase: specific observation of the rotating c subunit oligomer of EF<sub>0</sub>EF<sub>1</sub>. *FEBS Lett.* 472:34–38.
- Weiner, M. P., G. L. Costa, W. Schoettlin, J. Cline, E. Mathur, and J. C. Bauer. 1994. Site-directed mutagenesis of double-stranded DNA by the polymerase chain reaction. *Gene*. 151:119–123.
- Klionsky, D. J., W. S. A. Brusilow, and R. D. Simoni. 1984. In vivo evidence for the role of the epsilon subunit as an inhibitor of the proton-translocating ATPase of *Escherichia coli*. *J. Bacteriol.* 160:1055–1060.
- Wise, J. G. 1990. Site-directed mutagenesis of the conserved beta subunit tyrosine 331 of *Escherichia coli* ATP synthase yields catalytically active enzymes. *J. Biol. Chem.* 265:10403–10409.
- Sedmak, J. J., and S. E. Grossberg. 1977. A rapid, sensitive, and versatile assay for protein using Coomassie brilliant blue G250. *Anal. Biochem.* 79:544–552.
- Pardee, J. D., and J. A. Spudich. 1982. Purification of muscle actin. *Methods Enzymol.* 85:164–170.
- Vriend, G. 1990. WHAT IF: a molecular modeling and drug design program. *J. Mol. Graph.* 8:52–56.
- Jones, T. A., J. Y. Zou, S. W. Cowan, and M. Kjeldgaard. 1991. Improved methods for binding protein models in electron density maps and the location of errors in these models. *Acta Crystallogr. A*. 47:110–119.
- Cherepanov, D. A., and W. Junge. 2001. Viscoelastic dynamics of actin filaments coupled to rotary F-ATPase: curvature as an indicator of the torque. *Biophys. J.* 81:1234–1244.
- Pänke, O., D. A. Cherepanov, K. Gumbiowski, S. Engelbrecht, and W. Junge. 2001. Viscoelastic dynamics of actin filaments coupled to rotary F-ATPase: torque profile of the enzyme. *Biophys. J.* 81:1220–1233.
- Muller, M., K. Gumbiowski, D. A. Cherepanov, S. Winkler, W. Junge, S. Engelbrecht, and O. Panke. 2004. Rotary F<sub>1</sub>-ATPase. Is the



- C-terminus of subunit gamma fixed or mobile? *Eur. J. Biochem.* 271:3914–3922.
39. Sabbert, D., S. Engelbrecht, and W. Junge. 1996. Intersubunit rotation in active F-ATPase. *Nature.* 381:623–625.
40. Stock, D., A. G. Leslie, and J. E. Walker. 1999. Molecular architecture of the rotary motor in ATP synthase. *Science.* 286:1700–1705.
41. Bianchet, M., X. Ysem, J. Hullihen, P. L. Pedersen, and L. M. Amzel. 1991. Mitochondrial ATP synthase—quaternary structure of the F<sub>1</sub> moiety at 3.6 Å determined by x-ray diffraction analysis. *J. Biol. Chem.* 266:21197–21201.
42. Bianchet, M. A., J. Hullihen, P. L. Pedersen, and L. M. Amzel. 1998. The 2.8-Å structure of rat liver F<sub>1</sub>-ATPase: configuration of a critical intermediate in ATP synthesis/hydrolysis. *Proc. Natl. Acad. Sci. USA.* 95:11065–11070.
43. Groth, G., and E. Pohl. 2001. The structure of the chloroplast F<sub>1</sub>-ATPase at 3.2 Å resolution. *J. Biol. Chem.* 276:1345–1352.
44. Careaga, C. L., and J. J. Falke. 1992. Structure and dynamics of *Escherichia coli* chemosensory receptors. Engineered sulfhydryl studies. *Biophys. J.* 62:209–216.
45. Careaga, C. L., and J. J. Falke. 1992. Thermal motions of surface alpha-helices in the D-galactose chemosensory receptor. Detection by disulfide trapping. *J. Mol. Biol.* 226:1219–1235.
46. Baylis, J. A., N. P. Le, M. K. al Shawi, and R. K. Nakamoto. 2004. Reaction order of three-site rotational catalysis in the F<sub>1</sub>-ATPase. *Biophys. J.* 86:468a. (Abstr.)
47. Weber, J., and A. E. Senior. 2004. Fluorescent probes applied to catalytic cooperativity in ATP synthase. *Methods Enzymol.* 380: 132–152.
48. Hirono-Hara, Y., H. Noji, M. Nishiura, E. Muneyuki, K. Y. Hara, R. Yasuda, K. Kinosita Jr., and M. Yoshida. 2001. Pause and rotation of F<sub>1</sub>-ATPase during catalysis. *Proc. Natl. Acad. Sci. USA.* 98:13649–13654.